Catalysis Today 143 (2009) 195–202

Contents lists available at ScienceDirect

Catalysis Today

journal homepage: www.elsevier.com/locate/cattod

Pd-based $(Ce,Zr)O_x$-supported catalysts: Promoting effect of base metals (Cr, Cu, Ni) in CO and NO elimination

Ana Iglesias-Juez [a,*], Ana B. Hungría [b], Arturo Martínez-Arias [c], James A. Anderson [d], Marcos Fernández-García [c,**]

[a] Chemistry and Catalysis Group, Department of Chemistry, Utrecht University, Sorbonnelan 16, F.A.F.C. Wentgebouw, 3584 CA Utrecht, The Netherlands
[b] Departamento de Ciencia de los Materiales e Ingeniería Metalúrgica y Química Inorgánica, Universidad de Cádiz, 11510 Puerto Real, Spain
[c] Instituto de Catálisis y Petroleoquímica, CSIC, Campus Cantoblanco, 28049 Madrid, Spain
[d] Surface Chemistry and Catalysis Group, Department of Chemistry, University of Aberdeen, AB24 3UE Scotland, UK

ARTICLE INFO

Keywords:
CO–NO elimination
Pd–M catalysts
In situ
XANES
DRIFTS
TWC

ABSTRACT

A series of Pd–M bimetallic three-way catalysts (M = Cr, Cu and Ni) supported on a $(Ce,Zr)O_x$ material has been characterized using a combination of X-ray diffraction and Raman spectroscopy, and employing *in situ* diffuse reflectance Fourier transform infrared and X-ray near-edge structure spectroscopies to analyse the redox and chemical processes taking place during light-off conditions under CO, NO and O_2. The catalytic behaviour of these bimetallic systems was strongly affected by the degree of interaction between the noble and base metals in the calcined state. Among the base metals tested, Ni appeared to exert the least influence over the noble metal state/behaviour after calcination and under reaction conditions. Cr and Cu appear to interact with Pd in the calcined state, leading to a reduction in the temperature at which Pd was converted to Pd(0) with simultaneous formation of a binary PdM alloy during the reaction run. At high temperature, these alloy phases evolved into pure metallic Pd(0) particles and, in the case of the Cu-containing catalyst, result in a strong interaction with the support. The catalytic performance of these three Pd–M systems in the CO and NO elimination reactions are correlated with the nature and properties of the oxidized and reduced Pd-containing phases which are present in each case.

1. Introduction

Three-way catalysts (TWC) have been widely used to diminish pollutant emissions from gasoline engine powered vehicles [1]. In recent years, typical TWC formulations have included Pd as the active metal, fluorite-type oxides, such as ceria–zirconia, as promoters and alumina as support as well as other minor components mainly present in order to enhance thermal stability [1,2]. A degree of controversy still exists with respect to the inclusion of alumina when ceria–zirconia is used as promoter [3]. Apart from deactivation problems related to ageing of the system and which may be of importance in defining the life-time of the system [1,2], recent experimental evidence suggests that the behaviour of Pd under reaction conditions is significantly different in ceria–zirconia (CZ) than in ceria–zirconia/alumina (CZA)-supported systems [3–5]. This would appear to arise from the different degree of interaction between the noble metal and size-limited/two-dimensional ceria–zirconia patches, typically present in CZA supports, or bulk-like, three-dimensional crystallites [4].

On the other hand, and in contrast with Rh [6], Pd-based catalysts display limitations with respect to their ability to reduce NO [3,6,7]. Modification of Pd by introduction of a second, cheaper metal would appear to offer a viable solution from both an economical and catalytical point of view [8]. As now well known, the resulting bimetallic catalyst may display special catalytic features not anticipated by simple interpolation of the reactivity of constituents. The main physico-chemical effects exerted by the second metal on the noble metal component allow a simple classification of bimetallic systems. First of all, catalysts are found where the introduction of the second metal (M) may generate a binary phase, either in the oxidized and/or reduced chemical states. This is the case of Cu [9,10] or Cr [11,12]. A classic explanation of the differential behaviour with respect to the monometallic Pd system makes use of the interrelated structural (ensemble) or electronic (ligand) effects [13]. Structural effects are related to the generation or removal of certain surface sites while electronic ones are more subtle and induce changes in surface

* Corresponding author. Tel.: +31 62 865 1743; fax: +31 30 253 6760.
** Corresponding author.
E-mail addresses: A.IglesiasJuez@uu.nl (A. Iglesias-Juez), mfg@icp.csic.es (M. Fernández-García).

0920-5861/$ – see front matter © 2009 Elsevier B.V. All rights reserved.
doi:10.1016/j.cattod.2008.12.013

valence states. The second class of bimetallic systems may present modified behaviour as a consequence of the new "Pd" interface with the reactants. This may occur if the interaction of the second metal with the promoter or support is stronger [10], in turn not only by modifying the initial state of the noble metal, but also by forming new interfaces between Pd and this new component. The latter in particular affects the catalytic behaviour when a Pd(0)–M^{n+} interface with redox capabilities (of the second metal) is created, as may be expected in the case of Pd–Cr [12], Pd–Mo [14,15] and Pd–Mn [16] catalysts. This second class of systems is able to create new surface active sites for reaction or to block some Pd sites which are present in the reference Pd system.

It is therefore clear that a wide range of physico-chemical effects may influence the catalytic activity of Pd in TWCs by the addition of a second metal. The presence of a promoter with redox capabilities gives additional complexity to the system. In this work we analyse the influence of a second metal M on Pd/ZC performance for CO and NO elimination processes. To this end, we have chosen three base metal, M = Cr, Ni, and Cu, with the aim of covering the widest range of Pd–M interactions. While Cu and Cr may form stable mixed oxides with Pd [12,17], the three base metals may form binary Pd–M alloys [9–12,18]. Differences may however be encountered with the second metal miscibility in a zero-valent Pd fcc-matrix [18]. Additionally, the presence of a Pd–CrO_x interface has been claimed to affect catalytic activity [12]. The present Pd–M/CZ systems have been studied by using a multi-technique approach involving XRD, TEM–XEDS, and Raman for catalyst characterization and catalytic activity in combination with *in situ* DRIFTS and XANES techniques to evaluate the catalytic performance and its physico-chemical background.

2. Experimental

2.1. Catalyst preparation

A ceria–zirconia (CZ) support was prepared by using a microemulsion method; full details of the procedure can be found elsewhere [19]. After drying overnight at 373 K, this support was calcined under air at 773 K for 2 h (S_{BET} = 92 $m^2\ g^{-1}$). According to ICP-AES chemical analysis, it has a Zr/Ce atomic ratio of 1.0 ± 0.1. The bimetallic catalysts PdMCZ (M = Cr, Ni and Cu) were prepared by coimpregnation (incipient wetness method) of CZ support with aqueous solutions of palladium (II) and the second metal (copper(II), nickel(II), or chromium (III)) nitrates, from Alfa Aesar and Merck; purities > 99.99%) in an amount to give 1.0 wt.% of each of both the precious metal and the base metal. Monometallic references containing 1 wt.% of Pd or M (M = Cr, Ni and Cu) were also prepared. The catalysts were dried overnight at 373 K and calcined at 773 K for 2 h, and are referred to as PdCZ, CrCZ, NiCZ, CuCZ, PdCrCZ, PdNiCZ, and PdCuCZ.

2.2. Catalytic tests

Catalytic tests using stoichiometric mixtures of 1% CO + 0.45% O_2 + 0.1% NO (N_2 balance) at 30,000 h^{-1} were performed in a Pyrex glass flow reactor system. Details of the experimental conditions employed for these tests can be found elsewhere [4]. Gases were regulated with mass flow controllers and analysed using an on-line Perkin-Elmer 1725X FTIR spectrometer coupled with a multiple reflection transmission cell (Infrared Analysis Inc.; 2.4 m path length). Oxygen concentrations were determined using a paramagnetic analyser (Servomex 540A). Experimental error in the CO and/or NO conversion values obtained in these conditions is estimated as ±7%. Prior to catalytic testing, *in situ* calcination was performed with diluted oxygen (2.5% O_2 in N_2) at 773 K, followed by cooling under the same atmosphere and subsequent N_2 purging at room temperature (RT). A typical test consisted of increasing the temperature from 298 to 823 K at 5 K min^{-1}.

2.3. Characterization techniques

Powder X-ray diffraction (XRD) patterns were recorded on a Siemens D-500 diffractometer using nickel-filtered Cu Kα radiation operating at 40 kV and 25 mA and with a 0.025° step size. The line parameters of the patterns (position (2θ), FWHM, β, and shape) were obtained by the profile-fitting program ANALYZE (RayfleX version 2.293) supplied by Pantak Seifert Gmbh & Co. The line profiles were approximated by a pseudo-Voight function and the background level was determined using β-spline curves through the lower intensity points in the total patterns.

Transmission electron microscopy (TEM) analysis of materials was done with a JEOL 200 FX (0.31 nm point resolution) equipped with a LINK (AN10 000) probe for energy dispersive X-ray spectroscopy (XEDS).

Raman spectra were acquired using a Renishaw Dispersive system 1000, equipped with a single monochromator, a holographic Notch filter and a cooled TCD. Samples were excited using the 415 nm Ar laser line in an *in situ* cell (Linkam TS-1500), which allowed treatment under controlled atmospheres. Samples were analysed as stored and after drying at 773 K using synthetic air; spectra consisted of 100 accumulations during 15 min acquisition time, using a typical running power of 25 mW.

Diffuse reflectance infrared Fourier transform spectroscopy (DRIFTS) analysis of adsorbed species present on the catalyst surface under reaction conditions was carried out using a Perkin-Elmer 1750 FTIR fitted with an MCT detector. On-line analysis of the NO conversion at the outlet of the IR chamber was performed by chemiluminescence (Thermo Environmental Instruments 42C). Additional on-line gas analysis was performed using a Baltzers Prisma Quadrupole mass spectrometer. The DRIFTS cell (Harrick) was fitted with CaF_2 windows and a heating cartridge that allowed samples to be heated to 773 K. Samples of *ca.* 80 mg were calcined *in situ* at 773 K (with synthetic air, 20% O_2 in N_2) and then cooled to 298 K in synthetic air before introducing the reaction mixture and subsequently heating at 5 K min^{-1} up to 673 K, recording one spectrum (4 cm^{-1} resolution, average of 20 scans) generally every 10–15 K. The gas mixture (using the same concentrations as those employed for laboratory reactor tests) was prepared using a computer-controlled gas-blender with 75 $cm^3\ min^{-1}$ passing through the catalyst bed.

X-ray absorption near edge structure (XANES) experiments at the Pd K-edge were performed at the BM29 line of the ESRF synchrotron at Grenoble. A Si(1 1 1) monochromator, detuned at 50% to minimize harmonic content of the beam, and ionization chambers filled with Kr/Ar were used to obtain the transmission XAFS data. A Pd foil between the second and a third ionization chamber was measured simultaneously to calibrate the energy scale. Samples as self-supported discs (absorbance 0.5–2.0) were placed in a controlled-atmosphere cell for treatment. XANES spectra were taken every 15 K during a 5 K min^{-1} temperature ramp up to 673 K in the presence of the CO + NO + O_2 flowing mixture (similar to that employed for catalytic activity tests).

Results obtained in XANES experiments were subjected to normalization using standard procedures and analysed using principal component analysis (PCA) [20–23] which assumes that the absorbance in a set of spectra can be mathematically modelled as a linear sum of individual components, called factors, which correspond to each one of the palladium species present in a sample, plus noise [23]. To determine the number of individual components, an *F*-test based on the variance associated with factor *k* and the summed variance associated with the pool of noise factors is performed. A factor is accepted indicating the presence of

"real" chemical species (i.e. a factor associated with signal and not with noise) when the percentage of significance level of the *F*-test, %SL, is lower than a test level set in previous studies at 5% [20,21]. The ratio between the reduced eigenvalues, $R(r)$, which approaches one for noise factors, was also used in determining the number of factors. Once the number of individual components was set, XANES spectra corresponding to individual Pd species and their concentration versus temperature profiles were generated by an orthogonal rotation (varimax rotation) which should align factors (as close as possible) along the unknown concentration profiles, followed by iterative transformation factor analysis (ITFA). ITFA starts with delta function representations of the concentration profiles, associated with each chemical species, located at temperatures predicted by the varimax rotation, which are then subjected to refinement by iteration until error in the resulting concentration profiles is lower than the statistical error extracted from the set of raw spectra [20–22].

3. Results

The CO and NO conversion profiles for Pd and Pd–M catalysts are presented in Fig. 1A and B, respectively. Of the Pd-free samples, only CuCZ has been included in the plots as the remaining MCZ catalysts display zero activity below 500 K (CO) or 573 K (NO). CO oxidation proceeds at a lower temperature than NO reduction over all PdMCZ samples and is almost complete by 423 K. Among the bimetallic systems, only PdCuCZ displays a light-off profile for CO conversion which was shifted to lower temperatures compared to the remaining systems, with a modest decrease of about 25 K at 50% conversion (T_{50}; Table 1).

Below 370 K, conversion of NO corresponds to adsorption/desorption phenomena, producing negative conversion values for PdCuCZ and PdCrCZ. The case of PdNiCZ is different however, with some net conversion at low temperatures with a maximum at 375 K. PdCZ presents also similar feature to the later one showing a maximum at lower temperatures at 353 K. At high temperatures, above 420 K, PdCZ and PdNiCZ catalysts showed similar behaviour for NO conversion with T_{50} values at 445 and 448 K, respectively. The addition of Cr appeared to have a positive influence on the PdCZ system with a decrease in T_{50} by *ca.* 70 K (Table 1). Cu, on the other hand, shows a more erratic behaviour, giving conversion from 373 K and displaying a plateau between *ca.* 400 and 473 K, after which full conversion was only attained above *ca.* 573 K. The last part of the NO conversion profile seems dominated by the Cu component alone, as the bimetallic PdCuCZ sample displayed values equal to those of the CuCZ reference. For PdCuCZ, the T_{50} value was about 505 K (Table 1). NO_2 was never detected after contact of the reaction mixture with the samples. Regarding N-selectivity of the reduction process, a N_2O maximum below roughly 30% was obtained for all catalysts at temperatures below full conversion. 100% selectivity to N_2 was reached around 25 K beyond the temperature at which full NO conversion was achieved for all systems (Fig. 1).

Calcined samples were characterized by XRD and TEM–XEDS. In brief, XRD/TEM results mainly reflect information concerning the ceria–zirconia (CZ) components with no significant differences being noted when comparing the PdMCZ samples analysed here and the monometallic Pd reference sample reported earlier [4] or the CZ support alone [19]. According to these analyses, the CZ support component displays a Ce:Zr atomic ratio of ~1 (in agreement with chemical analysis), with an average crystallite size of 5 nm [19].

Pd mono- and bimetallic systems in a dehydrated state (dry air treatment at 523 K) present the Raman spectra shown in Fig. 2. Spectra are dominated by the band at 470 cm^{-1}, which together with a small band at 313 cm^{-1}, are known to pertain to a tetragonal

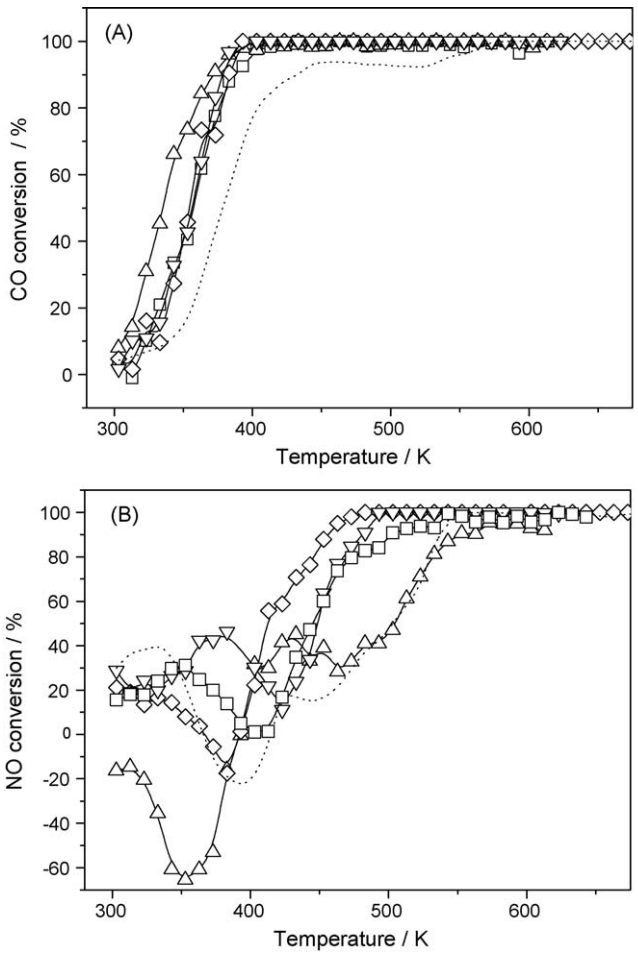

Fig. 1. CO (A) and NO (B) conversion profiles for the CO + NO + O_2 reaction over bimetallic Palladium–M samples and monometallic references. Squares, PdCZ; down-pointing triangles, PdNiCZ; diamonds, PdCrCZ; up-pointing triangles, PdCuCZ; dashed line, CuCZ.

Table 1
Temperatures (K) for CO and NO 50% conversion.

T_{50}	PdCZ	PdNiCZ	PdCrCZ	PdCuCZ
CO	357	357	354	335
NO	445	448	413	504

t″ CZ crystal phase (see Ref. [19] and references therein). A weak band at 523 cm^{-1}, present for PdCZ, is also related to this CZ phase [19]. All samples also display a band at 617 cm^{-1}. The latter can be assigned to the B_{2g} mode of PdO, since this material has a resonance enhanced Raman signal peaking at this energy [24]. Additional bands, only visible for PdCrCZ are detected at 990 and 840 cm^{-1} which are indicative of the presence of highly dispersed species (rather than well developed Cr-containing phases) and ascribed to terminal Cr=O and bridging Cr–O–Cr vibrations of Cr(VI) species in the form of chromates with a moderate degree of oligomerization [25–27].

Factor Analysis of the XANES data taken at the Pd K-edge (Table 2) gives evidence for the presence of two Pd-containing species for PdCZ and PdNiCZ and three for PdCuCZ and PdCrCZ. In some cases, the cut-off values for the %SL and $R(r)$ may indicate a possible (even if with low probability) third (PdNiCZ) or fourth (PdCuCZ and PdCrCZ) component which, however, can be dismissed by using more elaborated tests such as evolving factor

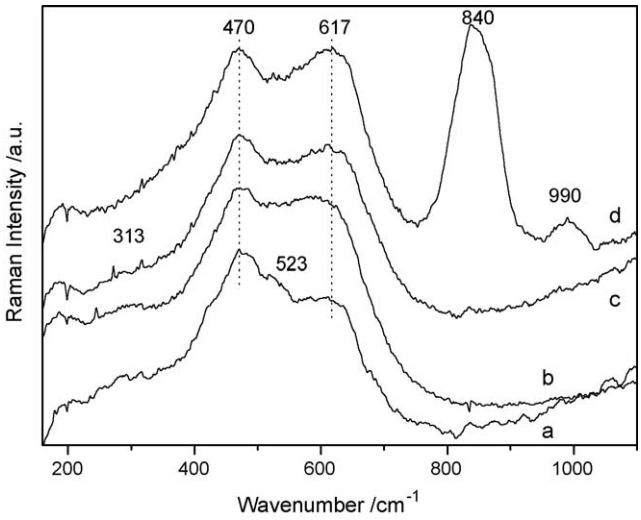

Fig. 2. Raman spectra of PdCZ (a), PdNiCZ (b), PdCuCZ (c) and PdCrCZ (d) samples.

analysis [22]. Concentration variation profiles for the two Pd-containing species extracted by ITFA for PdCZ and PdNiCZ are shown in Fig. 3A. A similar evolution under the reaction mixture is evident from this plot for both cases, with the maximum rate of initial Pd species disappearance around 460 K. The profiles corresponding to the two samples, PdCuCZ and PdCrCZ, having three Pd-containing compounds are included in Fig. 3B. Their

Table 2
Principal component analysis of Pd K-edge XANES results.

Factor	Eigenvalue	%SL	*R*(r)	Variance
A. PdCZ				
1	522.11	0.00	2534.1	99.962
2	0.19096	0.00	74.53	0.037
3	0.003236	6.02	2.36	0.001
4	0.00091	17.71	0.98	
5	0.00084	13.71	2.10	
6	0.00037	28.22	1.15	
7	0.00028	31.20	1.04	
8	0.00024	31.93	1.06	
B. PdNiCZ				
1	544.38	0.00	1432.1	99.933
2	0.35417	0.00	93.53	0.065
3	0.00350	4.93	2.71	0.001
4	0.00118	18.69	1.27	
5	0.00084	21.77	1.42	
6	0.00054	28.99	1.00	
7	0.00049	27.98	1.11	
8	0.00039	29.74	1.27	
C. PdCuCZ				
1	643.99	0.00	418.34	99.975
2	1.4322	0.00	131.25	0.223
3	0.01013	0.62	3.95	0.002
4	0.00237	8.68	2.38	0.001
5	0.00091	23.74	1.25	
6	0.00066	28.07	1.12	
7	0.00053	30.28	1.01	
8	0.00048	29.82	1.19	
D. PdCrCZ				
1	572.38	0.00	2363.45	99.958
2	0.22623	0.00	39.3	0.040
3	0.00534	2.40	1.99	0.001
4	0.00247	5.01	1.52	
5	0.00150	5.57	2.80	
6	0.00049	21.27	1.40	
7	0.00032	28.09	1.24	
8	0.00023	33.06	1.01	

Variances lower than 10^{-3} are not reported.

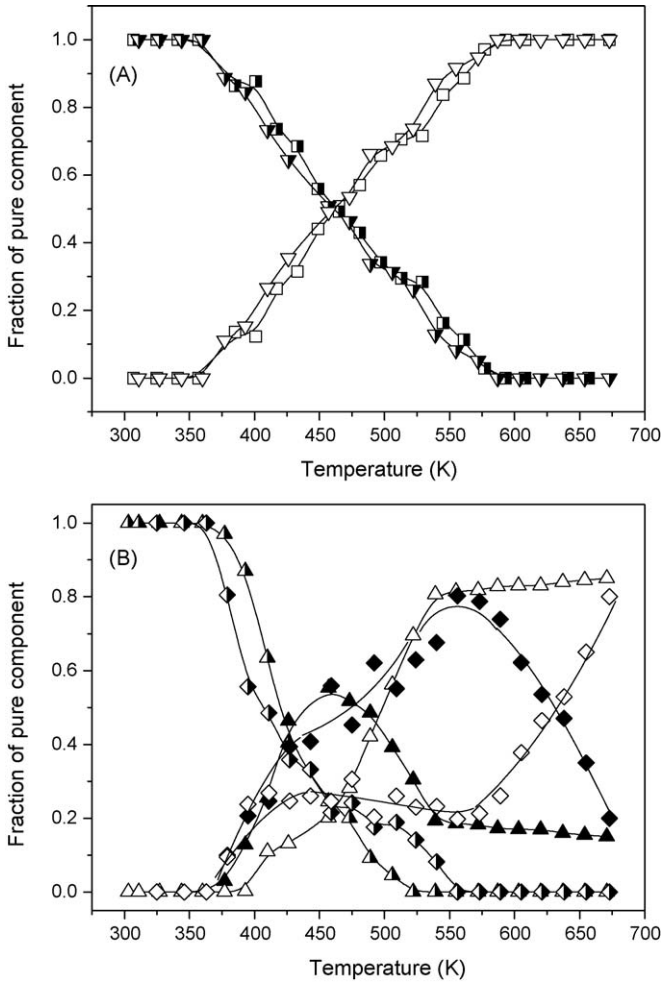

Fig. 3. Concentration profiles during the temperature-programmed reaction run for Pd-containing species of PdCZ (squares) and PdNiCZ (down-pointing triangles) (A) and PdCrCZ (diamonds) and PdCuCZ (up-pointing triangles) samples (B). Initial species (half-filled symbols); intermediate species (filled symbols), and final species (open symbols).

initial species evolve earlier than those of the other Pd systems (maximum disappearance rate at 405 and 420 K for PdCrCZ and PdCuCZ, respectively). They also share the common features of both presenting an intermediate which coexist with the final Pd phase almost from the onset. The intermediate species reached a maximum concentration at *ca.* 455 and 555 K for PdCuCZ and PdCrCZ, respectively. Finally, above 650 K, final Pd-containing species predominated for all catalysts.

The Pd XANES spectra associated with the concentration profiles are depicted in Fig. 4. Fig. 4A displays the spectra of the initial species, which can be ascribed to different Pd(I) or Pd(II) oxidation states by their edge position [22] and by comparison with the PdO reference. PdCZ and PdNiCZ species have a XANES spectra with the edge shifted to lower energy and with diminished intensity for the 5sp continuum resonance (CR) at *ca.* 24,365 eV when compared with the PdO reference. Both facts clearly indicate a partial reduction of the initial Pd species (which immediately after calcination is PdO-like—result not shown) to an average Pd(I)-like state by influence of the reactive atmosphere. Such an influence is the consequence of the CZ support properties, as the same metal component supported on pure alumina does not show significant differences from the PdO reference XANES spectrum after contact with the reactive mixture [28]. The influence on the initial Pd phase is less important for PdCrCZ and almost negligible

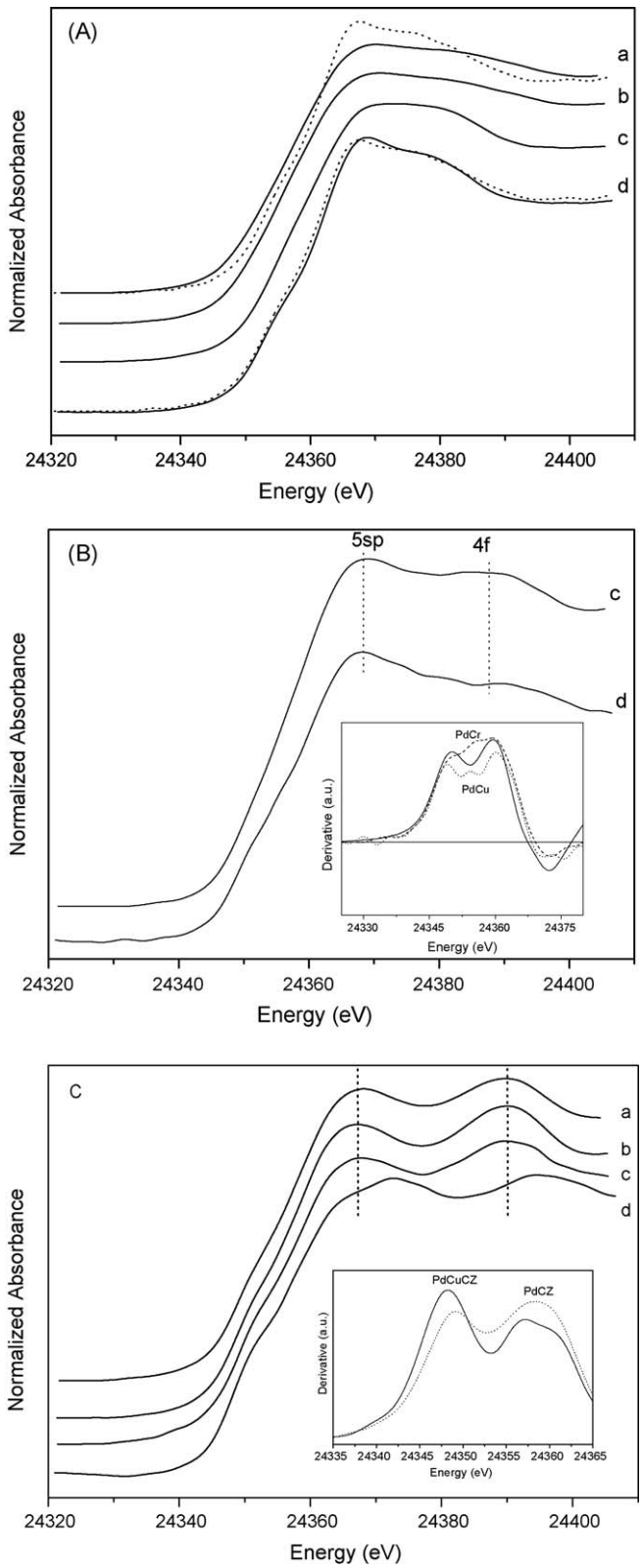

Fig. 4. XANES spectra for PCA predicted chemical species. (A) Pd initial, oxidized species; (B) Pd intermediate species; (C) Pd final, reduced species. Inset in B and C shows the derivative of XANES spectra and Pd foil (full line, B). Lower case labels (a) PdCZ (b) PdNiCZ, (c) PdCrCZ, (d) PdCuCZ. Reference compound, PdO, as doted line.

for PdCuCZ. In the latter case, since Pd(II) species present in PdCZ after calcination gives rise to Pd(I) species upon contact with CO + NO + O_2, we can presume that the oxidized phase present is a Pd–Cu binary oxide, which has the same Pd local geometry as PdO (D_{2h}) and therefore displays a very similar XANES spectrum [30]. Alternatively, modification of the CZ properties by the Cr or Cu component could also account for the different behaviour of the noble metal with respect to the monometallic PdCZ reference.

The XANES spectra of the intermediate species are shown in Fig. 4B together with their derivatives at the edge region (inset). Comparison of the latter curves with that corresponding to Pd foil clearly indicates a zero-valent state of Pd in such chemical matrixes [22]. In fact, the XANES shape displayed by both Pd-containing intermediate species is close to that reported for Pd–Cu alloys with an atomic ratio close to 1:1 [17]. This allows a clear assignment of the PdCuCZ intermediate species to such an alloy. To our knowledge, no previous report exists on PdCr alloy Pd K-edge XANES spectra; however, analysis of results obtained for the Pd L_{III}-edge on these materials [31] evidences similar (moderate) electronic/geometric perturbation of the Pd fcc-matrix due to the effect of alloying with either Cu or Cr, thus giving support to the assignment of the zero-valent intermediate phase to a PdCr alloy. For bulk PdCr alloys, the solubility limit of Cr into a Pd fcc-matrix is *ca.* 15 at.% [32]. Although the situation for small particles may be different, this may well limit the Cr:Pd atomic ratio ascribable to the intermediate species detected in PdCrCZ. It is important to stress that both alloy species are unstable, decomposing to give a final Pd(0)-species above 450 K (PdCuCZ) and 550 K (PdCrCZ).

The XANES spectra of the final Pd-species obtained for all samples are depicted in Fig. 4C. For PdCZ, PdNiCZ and PdCrCZ the XANES shape is readily ascribable to a Pd(0) species. Small differences among samples, here restricted to the intensity of the 5sp (*ca.* 24,365 eV) and 4f (*ca.* 24,395 eV) CRs, can be explained on the basis of moderate variations in particle size, which, on the other hand, appears to be lower (considering the lower height and larger width of the CRs [33]) for the PdCrCZ system and very similar for the other two systems. The only catalyst presenting noticeable differences in the XANES shape of the Pd-containing final species is PdCuCZ. Although the edge position and CR characteristics allow an assignment to a zero-valent Pd(0) species in a fcc-like matrix [22], no clear attribution can be made. Differences with the typical pure metal XANES spectrum (as those displayed by the other samples) concern the shift to higher energy visible for the 5sp and 4f CRs as well as a significant increase in the density of empty states close to the Fermi edge (*ca.* 24,350–60 eV). The edge derivative displayed in the inset of Fig. 4C confirms the above mentioned differences described in the Fermi region. The first point, e.g. energy shift of CRs, could be justified on the basis of a 2D, planar-like morphology for the Pd particle [33] while the second strongly suggests a contribution from the Ce 4f states [34,35] as cerium is the only cation among those present (Cr, Ce and Zr) which can give significant density of empty states close to the Fermi edge of Pd. Both facts could be understood by considering the formation pathway of the Pd particles (see below).

DRIFTS spectra recorded under the CO + NO + O_2 mixture for PdCZ, PdNiCZ, PdCuCZ and PdCrCZ samples are shown in Fig. 5. All catalysts except PdCuCZ display main bands at *ca.* 2155 and 2130 cm^{-1} after contact with the reaction mixture at room temperature. These bands are indicative of the presence of oxidized Pd^{n+} centres at the surface of the material [4,5,9–13,36]. A contribution at or close to 2110 cm^{-1}, attributed to carbonyls on Pd(I) centres [4,5,9–13,34], appeared as a shoulder of those main bands. Also very weak bands due the formation of metallic Pd carbonyls can be inferred at 2090–2040 and 1975–1900 cm^{-1} regions and ascribed to lineal and bridge-bonded species, respectively [4,5,9–13]. When the temperature ramp was initiated, the evolution of features for the three systems PdCZ, PdNiCZ, and PdCrCZ was similar. All carbonyl species disappear above 483 K. The PdCuCZ, on the other hand, displays larger IR band intensity than the other catalysts (note the multiplication

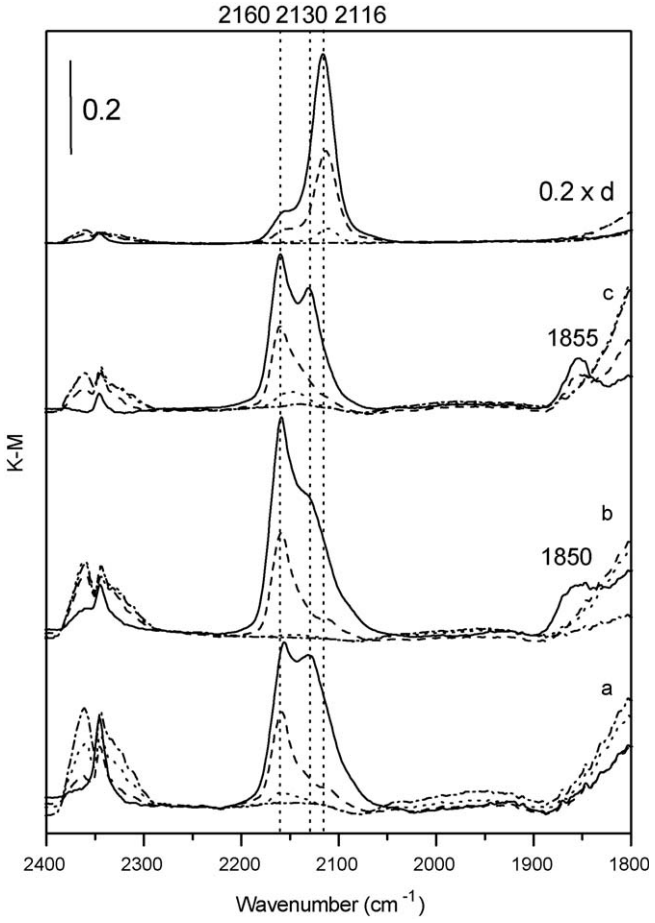

Fig. 5. DRIFTS spectra of (a) PdCZ, (b) PdNiCZ, (c) PdCrCZ and (d) PdCuCZ samples in a flow of 1% CO, 0.45% O_2, 0.1% NO, N_2 balance at 303 K (full line), 393 K (dashed line), 423 K (dotted line), and 483 K (dashed-dotted line).

factor used in Fig. 5 for PdCuCZ) and is dominated at RT by a contribution at 2116 cm^{-1}, assigned to Cu(I) carbonyl species and typically detected in Cu-containing CZ-supported samples [10]. The above mentioned Pd^{n+} carbonyls are also visible in this sample and show a thermal stability similar to that of the other catalysts.

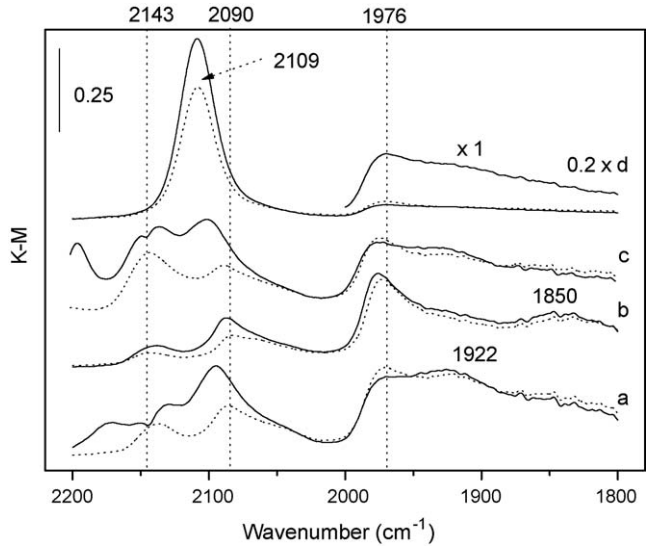

Fig. 6. DRIFTS spectra following experiments shown in Fig. 5 after exposure to CO (full lines) and subsequent flushing with N_2 (dashed lines). (a) PdCZ, (b) PdNiCZ, (c) PdCrCZ, and (d) PdCuCZ.

Minor bands at 1850–55 cm^{-1} ascribed to NO–Ni(II) (PdNiCZ) and NO–Pd(0) (PdCrCZ), were detected occasionally at low temperatures and assigned on the basis of similar experiments performed on monometallic PdCZ and MCZ reference systems.

To examine the state of the metal surfaces at the end of the reaction runs and in the absence of thermally driven adsorption effects, samples were flushed at 673 K and cooled in N_2 to room temperature and subsequently exposed to 1% CO/N_2 before again flushing the cell with N_2. Spectra recorded during this treatment are displayed in Fig. 6. Again strong similarities are apparent between PdCZ and PdNiCZ and to a lesser extent for PdCrCZ. In these three samples, bands at/around 2090, 1975 and *ca.* 1925/1850 cm^{-1}, ascribed to on-top, bridge and three-fold Pd(0) carbonyls, respectively, coexist with a band at 2143 cm^{-1}, characteristic of the presence of surface Pd(II) centres [4,5,9–13,34]. The latter appeared with greater intensity for PdCrCZ. The spectrum for PdCuCZ was, on the other hand, dominated by the band due to a CO–Cu(I) complex [10] while Pd(II) and three-fold Pd(0) contributions were probably absent as they are observed with strongly diminished intensity.

4. Discussion

4.1. Palladium phase evolution under reaction conditions

All samples after calcination showed strong similarities in the Raman (Fig. 2) and XANES (data not shown) spectra in respect to the initial Pd species. The oxidized Pd compound displays, however, different behaviour when the reaction mixture interacts with its surface at room temperature. While PdCZ and PdNiCZ samples evolve to give a partially reduced Pd(I)-like species, the presence of Cr appears to control the evolution of Pd while Cu, apparently, completely blocks it. This can be rationalized on the basis of the Pd–promoter interface, which remains essentially unaltered in the presence of Ni but is partially blocked by oxidic Cr entities. Some of the oligomeric Cr(IV) species detected by Raman must then modify the CZ component or be in contact with Pd but without generating any oxidized binary phase. The case of Cu is better explained if the existence of a $Pd_xCu_yO_z$ mixed oxide is hypothesized. In any case, although a full explanation of the Pd–M interaction developed after calcination remains elusive, the close proximity of Cu and Cr to the noble metal is manifested by the XANES results.

These differences in the initial, oxidized Pd state strongly influence the evolution of Pd under the stoichiometric $CO + NO + O_2$ atmosphere. The lack of influence by Ni on the initial (oxidized) noble metal state agrees with the observation that the evolution of the Pd surface (Fig. 5) and bulk (Fig. 3A) states in PdNiCZ while heating under the reaction mixture is very similar to that presented by the monometallic system. On the other hand, an initial direct contact between PdO-like species and Cr(VI) oligomers is more likely to induce the generation of a PdCr alloy. This alloy is detected concomitantly with reduction of a portion of Pd to the metallic state which, apparently, is not strongly affected by the base metal. Both zero-valent Pd phases coexist during the light-off test but above 555 K the PdCr alloy destabilizes to give the final, metallic Pd(0) phase. A somewhat similar case is observed for PdCuCZ. In this catalyst, the formation of the PdCu mixed oxide also facilitates the formation of a binary alloy and, of course, of zero-valent pure Pd species at temperatures below those found for the other two systems (PdCZ and PdNiCZ). However, formation of the third Pd-containing species appears a little retarded with respect to the intermediate and could be interpreted in terms of 2D, raft-like Pd particles with some interaction with Ce ions of the support. Again, similar to the case of PdCrCZ, the alloy evolves above 450 K into the third, 2D-like, Pd(0) species. As the PdCr and

PdCu alloys are expected to be thermodynamically stable phases with respect to their corresponding zero-valent metals even for nanosized entities (see Ref. [37] and references therein), their rupture implies the formation of other unknown phases. It can be hypothesized that the PdM bond rupture is thus induced by the formation of (Cu,Cr)$CeZrO_x$ ternary mixed oxides, which are known to exist [38]. Of course, the existence of raft-like Pd(0) particles with strong interaction with the promoter can also add enthalpy-related arguments to the Pd–Cu heterometallic bond rupture and might be in the origin of the more facile rupture of the corresponding alloy. Differences between these two PdM alloy systems are thus mainly related to their ranges of existence/stability, PdCu being the first to evolve to give Pd(0) particles (Fig. 3B).

In summary, it appears that Cu and Cr are the base metals of this study which exert a greater influence on the behaviour of Pd. (i) In first instance, by decreasing the temperature at which zero-valent Pd species first appears and generating larger quantities of such species below 500 K. (ii) The generation of PdM alloys has also obvious electronic effects; formation of PdCu alloys induces a moderate gain/loss of Pd 5sp/4d electronic densities [39] which might slightly enhance CO activation but which strongly favours NO dissociation [40]. Such PdM alloy phases are unstable under reaction conditions at high temperatures breaking in the zero-valent Pd phase. This stability is significantly lower for PdCuCZ. (iii) At high temperature, the Pd(0) phases generated also show some differences with the other two PdCZ and PdNiCZ systems. It appears that both Cu and Cr decrease the Pd particle size, this being most significant in the case of Cu, where a strong influence of the support is suggested by the XANES results (Fig. 4C). Note that the small size of the (raft-like) Pd(0) particles formed for PdCuCZ is based not only on the XANES results (Fig. 4C) but also on the IR spectrum after CO adsorption (Fig. 6), which displays bridging carbonyls, typical of open faces, rather than three-fold and on-top species (the latter somewhat masked by the CO–Cu(I) contribution), exclusive to closed packed (1 1 1)-like facets [4,41]. Note, however, that Ni also has (a weak) influence in the noble metal; the DRIFTS data (Fig. 6) showing the lower intensity detected for Pd–carbonyl species for PdNiCZ compared to PdCZ while also the atop/bridge intensity ratio differs, suggesting a difference in Pd dispersion, being higher for the monometallic sample than for PdNiCZ. Further studies are required to definitively address this point.

4.2. CO oxidation and NO reduction

In Pd model systems, while the CO + O_2 reaction is essentially considered structure insensitive [41] the CO + NO reaction turns out to be structure sensitive [42]. A weak sensitivity to the structure can nevertheless be observed for small Pd particles in the first reaction, as the CO desorption (the determining rate-step) has a slight dependence on particle size [43]. The second reaction appears structure sensitive since NO dissociation and, in particular, N recombination (to give N_2) steps are favoured, for small and large Pd particles, respectively [42,44]. The situation is, however, more complex in the presence of a support with redox capabilities. As shown in several studies of cerium-containing promoters [4,5,44–47], the Pd–promoter interface enhances NO and O_2 dissociation, giving an additional structure-sensitive factor common to both reactions. All of these facts clearly indicate that the NO/O_2 competition established for the reductant is strongly affected by Pd particle size and morphology (the latter being influenced by the Pd–support interface) and that both types of reaction, but in particular the reduction of NO, are sensitive to geometrical details of the Pd phase.

In the present case, the addition of a base metal permits a modification of several important parameters related to the noble metal phase behaviour under reaction conditions and thus its catalytic performance for CO and NO elimination reactions. As can be deduced by comparing Figs. 1 and 4, the light-off curves for CO and, particularly, NO display more drastic changes in the presence of Cr and Cu but in the temperature region where they perturb the electronic and geometric characteristics of the zero-valent Pd phases. The Ni case is different and no appreciable physico-chemical effect was detected in the noble metal component. As detailed in Section 4.1, the physico-chemical characterization provides significant evidence to suggest a weak influence of Ni on the noble metal.

For all Pd-containing samples, CO oxidation occurs selectively with oxygen below 380 K (Fig. 1). On that range of temperatures the formation of a bulk zero-valent Pd phase can be observed above 355 K (Fig. 3). On the other hand, DRIFTS data provides evidence for the presence of on-top Pd(0) carbonyls below and up to 363 K (Fig. 5), suggesting that such surface centres might be responsible for the CO activation and subsequent oxidation in all of these systems. The enhanced CO oxidation shown by PdCuCZ can, at least partially, be ascribed to the presence of Cu(I) centres as detected by DRIFTS (Fig. 5), which have significant activity in this reaction as demonstrated by the CuCZ reference CO conversion profile (Fig. 1A). This suggests that in these catalysts, the second metal only exerts a marginal influence in the CO oxidation behaviour of Pd.

Regarding the NO reduction process, it can be first noted that Pd and PdNi catalysts display a net NO conversion with a local maximum below 400 K. As shown by Granger et al. [47], for Pd and PdNi, the maximum at low temperatures can be related with the oxygen handling properties of the Ce-containing support; this latter component may supply oxygen vacancies located at the metal–support interface where NO dissociation occurs at low temperatures [5,44–48]. The relatively facile reaction of Pd-adsorbed NO with CZ-based anion vacancies might lead to N–O bond breaking with the O-fragment filling the anion vacancy and the N adatom forming a nitride-like species on Pd (which from the position of carbonyl IR bands would appear as oxidized Pd). However a deactivation phenomenon is observed. This could be related to the small Pd particle size in these catalysts. Previous studies have shown that the N recombination step to give N_2 is favoured for large particles; small particles present bigger proportion of low coordinated sites giving high stable N_{ad} and thus causing the suppression of active centers for NO dissociation and therefore decreasing the activity by self-poisoning [42]. That would explain why in spite of detecting bulk Pd reduction by XANES (Fig. 3) almost no bands related to metallic carbonyls are observed by DRIFTS (Fig. 5) and however they are present in similar experiments carried out in absence of NO [4].

On the other hand, in the case of PdCrCZ, a clear correlation appears between the formation of the PdCr alloy and the chemical processes taking place above *ca.* 370 K (Figs. 1 and 3B). This alloy specie appears at lower temperatures than the metallic phase for Pd and PdNi samples. As mentioned above, a significant electronic effect can be presumed in the alloy, which would strongly affect the NO dissociation process [40] and thus its reduction. It is also probable that the N recombination steps are additionally affected by the presence of Cr at Pd surfaces. What is in any case clear, is that the PdCr alloy lowers significantly the NO light-off temperature. This phase destabilizes and evolves into metallic Pd (Fig. 3.). However, at the range of temperatures that occurs, the electronic/geometric characteristics of the zero-valent Pd phase are of lesser importance for the elimination reactions.

The Cu-containing catalyst displays strong similarities with Cr at the initial part of the NO light-off profile, which could again be attributed to the presence of the corresponding PdCu alloy.

However, a "low temperature" plateau in the NO conversion plot (Fig. 1B) is observed in the region of the maximum concentration of the PdCu alloy, after which the system displays poor performance with respect to PdCZ and seems dominated by the contributions of Cu-alone. Within the plateau region, a strong surface rearrangement of the alloy with Cu segregation to the outermost layers is expected prior to the rupture of the binary phase. Therefore, the presence of Cu at the surface of the active phase, even from the oxidized state (Pd–Cu mixed oxide) alters the metal–support interface (oxygen handling) properties with respect to the parent monometallic system, inhibiting NO reduction below 400 K and dominating catalytic activity above 450 K.

The interaction between Pd and the second metal, M, is strongly favoured for the CZ support with respect to alumina [28]. In similar alumina-supported systems, the interaction is restricted to the PdCr sample and only in the oxidized state, with formation of a Pd(I)–Cr(III) mixed oxide. This suggests that the second metal may have a potentially greater influence in the elimination of pollutants (particularly NO) for TWCs when a ceria–zirconia support is used instead of the more complex ceria–zirconia/alumina. Further analysis is currently being performed to elucidate this aspect.

5. Conclusions

The behaviour of a series of Pd–M bimetallic catalysts for CO oxidation and NO reduction processes has been tested and compared with that of monometallic Pd references. The catalytic properties display a strong dependence on the degree of interaction which exists between the metals in the calcined state. While no interaction is detected between Ni and Pd, Cr in the form of Cr(VI) oligomers seems to present interfacial contact with Pd while Cu appears to form a PdCu binary mixed oxide.

For CO oxidation with oxygen, the second metal plays no significant role except in the case of PdCuCZ where a beneficial effect was noted and mostly resulted from the presence of active Cu(I) species. The enhancement in Pd–Cr and Pd–Cu interactions under the reaction mixture above 370 K exerted a significant influence on NO reduction. The initial decrease in the onset of light-off by *ca.* 70 K is attributed in both cases to the previous formation of the corresponding zero-valent binary Pd alloy phases. Differences between these systems involve the stability and surface characteristics of the alloy, being the former significantly lower for PdCuCZ. A correlation was detected between the maximum concentration region of the PdCu alloy and the plateau in NO conversion displayed by the PdCuCZ sample, after which the NO reduction activity was dominated by Cu. Ni showed different behaviour for NO conversion. No apparent influence on Pd under reaction conditions was detected and a difference in the initial noble metal dispersion would account for the differences in catalytic results.

Acknowledgements

We thank the Comunidad de Madrid for grants received (to A.B. H. and A. I.-J.) with which this work has been carried out. We are also grateful to the scientific and technical staff at ESRF Synchrotron (BM29) for their help during the XANES experiments and Dr. M.A. Bañares for recording Raman data.

References

[1] E.S.J. Lox, B.H. Engler, in: G. Ertl, H. Knözinger, J. Weitkamp (Eds.), Environmental Catalysis, Wiley–VCH, 1999, p. 1.
[2] A. Trovarelli, Catal. Rev. Sci. Eng. 38 (1996) 97 (references therein).
[3] Z. Hu, C.Z. Wan, Y.K. Lui, J. Dettling, J.J. Steger, Catal. Today 30 (1996) 83.
[4] M. Fernández-García, A. Martínez-Arias, A. Iglesias-Juez, A.B. Hungría, J.A. Anderson, J.C. Conesa, J. Soria, Appl. Catal. B 31 (2001) 39.
[5] A. Martínez-Arias, M. Fernández-García, A. Iglesias-Juez, A.B. Hungría, J.A. Anderson, J.C. Conesa, J. Soria, Appl. Catal. B 31 (2001) 51.
[6] R. van Yperen, D. Lindner, L. Mubmann, E.S. Lox, T. Kreuzer, Stud. Surf. Sci. Catal. 116 (1998) 51.
[7] M. Skoglundh, H. Johansson, L. Löwendahl, K. Jansson, L. Dahl, B. Hirschauer, Appl. Catal. B 7 (1996) 299.
[8] B. Coq, F. Figueras, J. Mol. Catal. A 173 (2001) 117.
[9] M. Fernández-García, A. Martínez-Arias, C. Belver, J.A. Anderson, J.C. Conesa, J. Soria, J. Catal. 194 (2000) 385.
[10] A.B. Hungría, A. Iglesias-Juez, A. Martínez-Arias, M. Fernández-García, J.A. Anderson, J.C. Conesa, J. Soria, J. Catal. 206 (2002) 281.
[11] A. Elhamdaoui, G. Bergeret, J. Massardier, M. Primet, A.J. Renouprez, J. Catal. 148 (1994) 47.
[12] M. Fernández-García, A. Martínez-Arias, A. Iglesias-Juez, A.B. Hungría, J.A. Anderson, J.C. Conesa, J. Soria, J. Catal. 214 (2003) 220.
[13] J.A. Rodriguez, Surf. Sci. Rep. 24 (1996) 223.
[14] T.E. Hoost, G.W. Graham, M. Shelef, O. Alexeev, B.C. Gates, Catal. Lett. 38 (1996) 57.
[15] M. Schmal, M.A.S. Baldanza, M.A. Vannice, J. Catal. 185 (1999) 138.
[16] J.F. Trillat, J. Massadier, B. Morawek, H. Praliaud, A.J. Renouprez, Stud. Surf. Sci. Catal. 116 (1998) 103.
[17] M. Fernández-García, J.A. Anderson, G.L. Haller, J. Phys. Chem. 100 (1996) 16247.
[18] T.B. Massalki, 2nd ed., Binary Alloy Phase Diagrams, vol. 1, ASM International, USA, 1993.
[19] A. Martínez-Arias, M. Fernández-García, V. Ballesteros, L.N. Salamanca, C. Otero, J.C. Conesa, J. Soria, Langmuir 15 (1999) 4796.
[20] M. Fernández-García, C. Márquez-Alvarez, G.L. Haller, J. Phys. Chem. 99 (1995) 12565.
[21] C. Márquez-Alvarez, I. Rodríguez-Ramos, A. Guerrero-Ruiz, G.L. Haller, M. Fernández-García, J. Am. Chem. Soc. 119 (1997) 2905.
[22] M. Fernández-García, Catal. Rev. Sci. Eng. 44 (2002) 59.
[23] E.R. Malinowsky, Factor Analysis in Chemistry, Wiley, New York, 1991.
[24] J.R. McBridge, K.C. Kass, W.H. Weber, Phys. Rev. B 44 (1991) 5016.
[25] M.I. Zaki, N.E. Foudad, J. Leyrer, H. Knozinger, Appl. Catal. 21 (1986) 359.
[26] B.M. Weckhuysen, I.E. Wachs, J. Phys. Chem. B 101 (1997) 2793.
[27] B. Grzybowska, J. Sloczynski, R. Grabowski, K. Wcislo, A. Kozlowska, J. Stoch, J. Zielinski, J. Catal. 178 (1998) 687.
[28] A.B. Hungría, M. Fernández-García, J.A. Anderson, A. Martínez-Arias, J. Catal. 235 (2005) 262.
[30] J.A. Anderson, M. Fernández-García, G.L. Haller, J. Catal. 164 (1996) 477.
[31] Y.S. Lee, K.Y. Kim, Y.D. Chung, C.N. Whang, Y. Jeon, Appl. Phys. A 70 (2000) 59.
[32] D. Wang, J.D. Cleway, T.B. Flanegan, J. Alloys Comp. 325 (2000) 151.
[33] D. Bazin, J.J. Rehr, J. Phys. Chem. B 107 (2003) 12398.
[34] A. Vega, S. Bouarab, M.A. Khan, Phys. Rev. B 51 (1995) 4823.
[35] W. Scheider, S.L. Molodtsov, M. Ritcher, Th. Gantz, P. Engelmenn, C. Lauschat, Phys. Rev. B 57 (1998) 14930.
[36] A. Bensalem, J.C. Muller, D. Tessier, F. Bozon-Verduraz, J. Chem. Soc., Faraday Trans. 92 (1996) 3233.
[37] B. Hammer, J.K. Norskov, Adv. Catal. 45 (2001) 71.
[38] D. Terrible, A. Trovarelli, C. Leitenburg, A. Primavera, G. Dolcetti, Catal. Today 47 (1999) 133.
[39] M. Fernández-García, J.C. Conesa, A. Clotet, J.M. Ricart, N. López, F. Illas, J. Phys. Chem. B 102 (1998) 141.
[40] F. Illas, N. López, A. Clotet, J.M. Ricart, J.C. Conesa, M. Fernández-García, J. Phys. Chem. B 102 (1998) 8017.
[41] X. Xu, D.W. Goodman, J. Phys. Chem. 97 (1993) 7711.
[42] D.R. Rainer, M. Koranne, S.M. Vesecky, D.W. Goodman, J. Phys. Chem. B 101 (1997) 10769.
[43] J. Hoffman, I. Meusel, J. Hartmann, J. Libuda, H.-J. Freund, J. Catal. 204 (2001) 378.
[44] J.H. Holles, R.J. Davis, Th.M. Murray, J.M. Howe, J. Catal. 195 (2000) 193.
[45] M. Fernández-García, A. Martínez-Arias, L.N. Salamanca, J.M. Coronado, J.A. Anderson, J.C. Conesa, J. Soria, J. Catal. 187 (1999) 474.
[46] P. Bera, V. Jayaram, G.N. Subbana, M.S. Hegde, J. Catal. 196 (2000) 293.
[47] P. Granger, J.F. Lamonier, A. Aboukais, L. Leclercq, G. Leclercq, Top. Catal. 16/17 (2001) 89.
[48] A. Martínez-Arias, J. Soria, J.C. Conesa, X.L. Seoane, A. Arcoya, R. Cataluña, J. Chem. Soc., Faraday Trans. 91 (1995) 1679.